THE JOURNAL OF PHYSICAL CHEMISTRY B

pubs.acs.org/JPCB Article

Combining Lindblad Master Equation and Surface Hopping to Evolve Distributions of Quantum Particles

Published as part of The Journal of Physical Chemistry virtual special issue "Peter J. Rossky Festschrift".

Yi-Siang Wang, Parmeet Nijjar, Xin Zhou, Denys I. Bondar, and Oleg V. Prezhdo*

Cite This: *J. Phys. Chem. B* 2020, 124, 4326–4337 Read Online

ABSTRACT: Motivated by the need to study nonequilibrium evolutions of many-electron systems at the atomistic ab initio level, as they occur in modern devices and applications, we developed a quantum dynamics approach bridging master equations and surface hopping (SH). The Lindblad master equation (LME) allows us to propagate efficiently ensembles of particles, while SH provides nonperturbative evaluation of transition rates that evolve in time and depend explicitly on nuclear geometry. We implemented the LME-SH technique within real-time time-dependent density functional theory using global flux SH, and we demonstrated its efficiency and utility by modeling metallic films, in which charge-phonon dynamics was studied experimentally and showed an unexpectedly strong dependence on adhesion layers. The LME-SH approach provides a general framework for modeling efficiently quantum dynamics in a broad range of complex many-electron condensed-matter and nanoscale systems.

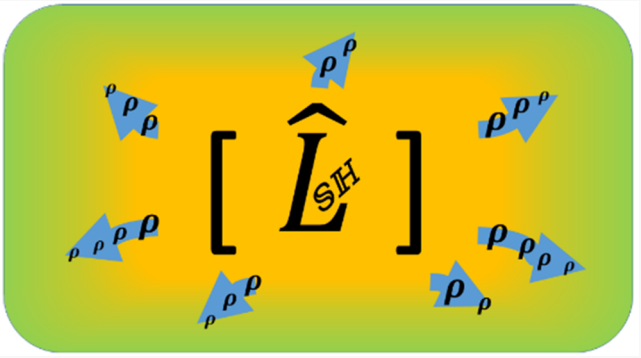

1. INTRODUCTION

Nanoscale systems can support multiple charge carriers that interact with each other and with phonons, forming more complex particles, such as polarons, excitons, trions, biexcitons, etc.[1−16] These particles can scatter off each other and exchange energy on ultrafast time scales, as measured by various time-resolved spectroscopies. Important examples of scattering processes involving large ensembles of particles include excitation of multiple electrons in semiconductors,[17,18] charge carrier equilibration, and cooling in metals initiated by excitation of surface plasmons,[6−8,14] Auger-type processes such as Auger-assisted charge trapping and recombination in 2D semiconductors,[19] multiple-exciton generation and annihilation in semiconductor quantum dots[5,9,10,13] and carbon nanotubes,[12] Auger-assisted electron transfer between quantum dots and molecules,[15] plasmon-driven electron transfer,[11,14] and carrier trapping and recombination in halide perovskites.[16,20,21] While particle−particle scattering occurs in condensed matter of any dimensionality, it is particularly important in nanoscale systems, in which quantum confinement brings particles closer to each other and reduces dielectric screening, at the same time maintaining high densities of states. The above processes are important in many applications, including electronics, spintronics, electro-optics, thermo-electrics, photovoltaics, and photocatalysis. They occur on ultrafast time scales in competition with each other, and they are actively studied by time-resolved experimental techniques, strongly motivating corresponding theoretical efforts.

The presence of multiple excitations makes *ab initio* modeling of the ultrafast scattering processes extremely challenging. The majority of theoretical efforts is limited to phenomenological and kinetic models, such as the two-temperature model[22,23] used to describe electron equilibration and relaxation in metals, and the kinetic models constructed to describe the dependence of carrier−carrier scattering, trapping and recombination on carrier density.[24−26] Real-time time-dependent density functional theory[27] (TDDFT) provides a rigorous formalism for studying excited state dynamics in condensed matter systems at the *ab initio* level. However, its application to systems involving multiple excitations is extremely challenging computationally. In addition, real-time TDDFT treats phonons classically, and coupling of the DFT electron density to classical atoms in a mean-field way, as in the

Received: April 5, 2020
Revised: May 1, 2020
Published: May 4, 2020

https://dx.doi.org/10.1021/acs.jpcb.0c03030
J. Phys. Chem. B 2020, 124, 4326–4337

quantum-classical Ehrenfest approach[28] implemented with TDDFT,[29−31] has problems achieving thermodynamic equilibrium. The Ehrenfest method works well for short-time dynamics, but has a hard time describing energy transfer from quantum mechanical electrons to classical phonons, required to achieve thermodynamics equilibrium in the long time limit.[32] Open system TDDFT[33] or nonequilibrium Green's function theory[34] can provide a framework to address this problem. Redfield-type theories provide an alternative description.[35] The Hamiltonian is separated into system (electrons) and environment (phonons), both of which are treated quantum mechanically. The system is assumed to be weakly coupled to the environment, and thus the interaction is treated perturbatively. Furthermore, vibrational motions are assumed to be harmonic, which is not the case, for example, with the highly anharmonic dynamics of halide perovskites[36,37] or in the photoexcited semiconductors undergoing phase transitions.[38−40] Redfield theory can describe energy dissipation and thermodynamics equilibration; however, due to perturbative treatment, the Redfield master equation can lose positivity of the density matrix. Closely related to the Redfield equation, the Lindblad master equation[41] (LME) preserves density matrix positivity.[42] Similar to the Redfield equation, it contains parameters that are often estimated perturbatively and/or phenomenologically, losing connection with the underlying microscopic description.

In order to describe accurately the coupled electron−phonon dynamics of nanoscale systems it is desirable to combine the features of real-time TDDFT and other quantum-mechanical methods, which treat the systems nonperturbatively and at the atomistic level, with those of master equations, which are capable of describing ensembles of particles and achieving thermodynamic equilibria. Surface hopping[28,43−51] (SH) provides the desired connection. Starting with a time-dependent Schrodinger equation, SH defines transition rates that are time-dependent, nonperturbative and depend on the current atomistic structure of a system. SH transition rates enter a master-type equation that is used to propagate an ensemble of systems including transitions between different quantum states.[51] The previous versions of SH,[28,44−51] including its implementation within real-time TDDFT,[52−55] solve the full quantum mechanical problem for the electronic evolution. Even in the case of only two-particle excitations in a nanoscale system containing a couple dozen atoms,[56] the number of states is huge, making such description impractical for large systems and many particle excitations. In this paper, we resolve this problem by using the nonperturbative atomistic SH transition rates in a Lindblad master equation for a Fermi−Dirac type distribution of excited electrons. The developed method is illustrated with phonon-induced relaxation of a charge carrier ensemble in metal films that are of interest in microelectronics, thermo-electrics and electro-optics[57−68] and that have been studied in recent experiments[69] using the time-domain thermo-reflectance technique.[70,71]

The following section describes the developed approach, combining the LME with global flux SH[72−74] (GFSH), and discusses connection between these two techniques. Section 3 introduces application of the LME-SH method to metal films, provides computational details, and describes the modeling results. Section 4 contains additional remarks and conclusions.

2. THEORY: LINDBLAD MASTER EQUATION WITH SURFACE HOPPING TRANSITION RATES

The methodology developed in this work combines the phenomenological LME for the evolution of a many-body quantum system with the nonperturbative atomistic SH evaluation of the rates of transitions between the states.

Traditional SH is based on solution of a Schrodinger or quantum Liouville−von Neumann equation, with dimensionality scaling exponentially with the number of particles. Therefore, traditional SH cannot be applied to systems containing large numbers of particles. At the same time, quantum transition rates obtained in SH depend explicitly on atomic evolution, which is very important if a system undergoes an atomic rearrangement, for instance, a defect diffusion in a metal halide perovskite.[75] Further, SH provides a back-reaction from the electrons to nuclei, which is critical, for instance, in photoinduced phase transitions.[38−40] The LME allows one to evolve efficiently particle distributions, and thus, it is easily applicable to studies of large ensembles of particles. However, transition rates entering the LME are usually independent of time. Therefore, traditional applications of the LME ignore dependence of electronic evolution on atomic motions and cannot generate the back-reaction. By applying the SH ideas to the LME, we are able to incorporate explicitly the coupling between electronic and atomic evolutions, while at the same time we are able to treat dynamics involving large numbers of quantum particles.

2.1. Lindblad and Pauli Master Equations. The LME[41,76,77] is often used to describe evolution of a many body system coupled to an environment (bath):

$$\frac{\mathrm{d}\hat{\rho}(t)}{\mathrm{d}t} = \frac{i}{\hbar}[\hat{\rho}(t), \hat{H}] + \sum_k \left(\hat{A}_k \hat{\rho}(t) \hat{A}_k^{\dagger} - \frac{1}{2}\hat{\rho}(t)\hat{A}_k^{\dagger}\hat{A}_k - \frac{1}{2}\hat{A}_k^{\dagger}\hat{A}_k\hat{\rho}(t) \right) \tag{1}$$

Here, $\hat{\rho}(t)$ and $\hat{H}$ are the density matrix and the Hamiltonian of the system in consideration, and $\hat{A}_k$ and $\hat{A}_k^{\dagger}$ are the transition operator and its complex conjugate, respectively, modeling interaction with the bath. A common choice for $\hat{A}_k$ and $\hat{A}_k^{\dagger}$ is the lowering and raising operators describing transitions between pairs of states in the system, induced by system-bath interactions. Coupling to the bath allows an out-of-equilibrium system to evolve toward equilibrium.[78] The transition operators can be weighted by the transition rate, γ. Under these assumptions, the Lindblad equation can be rewritten as

$$\begin{aligned}\frac{\mathrm{d}\hat{\rho}(t)}{\mathrm{d}t} = \frac{i}{\hbar}[\hat{\rho}(t), \hat{H}] &+ \sum_{k>j} \gamma_{k\to j}\left(\hat{A}_{k\to j}\hat{\rho}(t)\hat{A}_{k\to j}^{\dagger} - \frac{1}{2}\hat{\rho}(t)\hat{A}_{k\to j}^{\dagger}\hat{A}_{k\to j} - \frac{1}{2}\hat{A}_{k\to j}^{\dagger}\hat{A}_{k\to j}\hat{\rho}(t) \right) \\ &+ \sum_{k\le j} \gamma_{k\to j}\left(\hat{A}_{k\to j}\hat{\rho}(t)\hat{A}_{k\to j}^{\dagger} - \frac{1}{2}\hat{\rho}(t)\hat{A}_{k\to j}^{\dagger}\hat{A}_{k\to j} - \frac{1}{2}\hat{A}_{k\to j}^{\dagger}\hat{A}_{k\to j}\hat{\rho}(t) \right),\end{aligned} \tag{2}$$

where the transition operators are

$$\hat{A}_{k\to j} = |\Phi_k\rangle\langle\Phi_j| \text{ and } \hat{A}_{k\to j}^{\dagger} = |\Phi_j\rangle\langle\Phi_k| \tag{3}$$

https://dx.doi.org/10.1021/acs.jpcb.0c03030
J. Phys. Chem. B 2020, 124, 4326−4337

Let $|\Phi_n\rangle$ be eigenstates of the Hamiltonian $\hat{H}$. Hence,

$$\hat{H}|\Phi_n\rangle = E_n|\Phi_n\rangle, \text{ and } \langle\Phi_{n'}|\Phi_n\rangle = \delta_{n,n'} \tag{4}$$

where E_n is the energy of state $|\Phi_n\rangle$.

The goal of the present work is to evolve a distribution of an ensemble of quantum particles spread over multiple states $|\Phi_n\rangle$. Therefore, we focus on evolution of the state $|\Phi_n\rangle$ populations, $P_n(t) = \langle\Phi_n \mid \hat{\rho}(t) \mid \Phi_n\rangle$, given by the diagonal elements of the density matrix. Sandwiching eq 2 between the eigenstates $\mid \Phi_n\rangle$ and using eqs 3 and 4, one can obtain the Pauli master equation (PME),

$$\frac{\mathrm{d}\langle\Phi_n|\hat{\rho}(t)|\Phi_n\rangle}{\mathrm{d}t} = \frac{\mathrm{d}P_n(t)}{\mathrm{d}t} = \sum_j [\gamma_{n\to j}P_j(t) - \gamma_{j\to n}P_n(t)] \tag{5}$$

which describes a continuous-time Markov process. Here, P_n and P_j denote populations of states n and j, and $\gamma_{n\to j}$ and $\gamma_{j\to n}$ are rates of transition from state n to state j, and from state j to state n, respectively. In the current work, the transition rates will be determined from SH.

The motivation for the current work is provided by experiments performed on metallic and semiconducting systems involving ensembles of electrons. Electrons follow the Fermi−Dirac statistics and equilibrate to the Fermi−Dirac distribution defined as

$$P_n = \frac{1}{Z}\frac{1}{\mathrm{e}^{\beta(E_n-\mu)}+1} \tag{6}$$

where $\beta = \frac{1}{k_B T}$, k_B is Boltzmann constant, T is temperature, μ is chemical potential, and Z is the partition function. Plugging the Fermi−Dirac populations into the PME, eq 5, and requiring that they correspond to a stationary state leads to

$$\frac{dP_n(t)}{dt} = \sum_j \left[\gamma_{n\to j}\frac{1}{Z}\frac{1}{e^{\beta(E_j-\mu)}+1} - \gamma_{j\to n}\frac{1}{Z}\frac{1}{e^{\beta(E_n-\mu)}+1}\right] = 0. \tag{7}$$

In order to satisfy this equation, the rates of the forward and backward transitions should be related by the detailed balance condition,

$$\frac{\gamma_{n\to j}}{\gamma_{j\to n}} = \frac{\mathrm{e}^{\beta(E_j-\mu)}+1}{\mathrm{e}^{\beta(E_n-\mu)}+1} \tag{8}$$

The rate of transitions that lower electron energy will be defined by a SH formula. The rate of transitions upward in energy will be obtained from the downward transition rate and the state energies using eq 8.

Similar conditions relating the rates of transitions upward and downward in energy can be obtained for the Boltzmann−Gibbs and Bose−Einstein statistics. In particular, the Boltzmann−Gibbs detailed balance condition, $\gamma_{n\to j}/\gamma_{j\to n} = e^{-\beta(E_n - E_j)}$, is now commonly used to model quantum transitions with SH under the classical path approximation (CPA).[79,80]

2.2. Surface Hopping. SH is a family of nonadiabatic (NA) molecular dynamics (MD) techniques generalizing the more common adiabatic MD to include transitions between adiabatic states.[28,43,44,46−48] SH takes full advantage of the extremely powerful MD approaches capable of describing dynamics of large molecular, condensed matter, nanoscale and biological systems at the atomistic level. The traditional adiabatic MD restricts atomic evolution to a single potential energy surface associated with the given, typically ground, electronic state. In comparison, NAMD obtains probabilities of transitions between states, and switches atomic evolution from one electronic state to another, evolving the atoms on the potential energy surface associated with the currently occupied electronic state. In simple cases, one can use semiclassical expressions for transition probabilities, such as the Landau−Zener,[81] Nikitin,[82] Miller,[83] or Zhu−Nakamura equations.[84] In complex condensed matter systems, in which transitions cannot be tracked one-by-one and which cannot be approximated by simple one-dimensional models, transition probabilities are generated automatically on a computer, and Monte Carlo type stochastic algorithms are used to perform NAMD simulations. The vast majority of such SH schemes starts by solving the time-dependent Schrodinger equation for the wave function of the quantum (electronic) subsystem or the corresponding equation for the density matrix. Since the Lindblad equation deals with density matrices, we use the latter formulation.

2.2.1. Evolution of the Quantum Subsystem. Evolution of a density matrix of a closed system can be described by the quantum Liouville−von Neumann equation

$$\frac{\mathrm{d}\hat{\rho}(t)}{\mathrm{d}t} = \frac{i}{\hbar}[\hat{\rho}(t), \hat{H}(\mathbf{r}; \boldsymbol{R})] \tag{9}$$

where $\hat{H}$ is the Hamiltonian, and $\hat{\rho}$ is the density matrix. Atomic motions are treated in NAMD classically, and therefore, the quantum (electronic) Hamiltonian depends parametrically on classical atomic coordinates, $\boldsymbol{R}$. The separation of the electronic and atomic degrees of freedom arises from the vast difference in the time scales of electronic and atomic motions.

Formally, eq 9 is a unitary version of eq 1. The LME, eq 1, can be used to describe a quantum electronic subsystem coupled to a bath of quantum harmonic oscillators. It is used here as the starting point to obtain the PME, eq 5, which is used in the actual calculations according to the proposed approach. On the other hand, eq 9 describes a quantum electronic subsystem coupled to classical atoms undergoing arbitrary motions. Equation 9 is also used in the calculations, as part of a SH algorithm.

As before, we use the eigenstate representation, eq 4, to solve eq 9. Applying the adiabatic basis to eq 9,

$$\langle\Phi_n|\frac{\partial}{\partial t}\hat{\rho}|\Phi_j\rangle = \left(\frac{i}{\hbar}\right)\langle\Phi_n|\hat{\rho}\hat{H} - \hat{H}\hat{\rho}|\Phi_j\rangle, \tag{10}$$

we obtain evolution of the matrix elements of the density matrix

$$i\hbar\frac{\partial}{\partial t}\rho_{nj}(t) = \sum_l [\rho_{lj}(H_{jl} + d_{jl}) - \rho_{nl}(H_{\ln} + d_{\ln})] \tag{11}$$

The diagonal element, ρ_{nn}, represents population of state n, while the off-diagonal elements, ρ_{nj}, represent coherences.

The electronic Hamiltonian is diagonal in the eigenvalue representation,

$$H_{jl}(\mathrm{R}) = \langle\Phi_j|H|\Phi_l\rangle = E_j\delta_{j,l} \tag{12}$$

We keep the off-diagonal elements explicitly in eq 11, because the Φ_l used below are single-particle wave functions, and in later works, we may introduce interactions between particles,

https://dx.doi.org/10.1021/acs.jpcb.0c03030
J. Phys. Chem. B 2020, 124, 4326−4337

to account for not only electron−phonon but also electron−electron scattering.

The NA coupling

$$d_{lj} = -i\hbar \frac{\langle \Phi_l | \nabla_R H | \Phi_j \rangle}{E_j - E_l} \frac{d\boldsymbol{R}}{dt} = -i\hbar \langle \Phi_l | \nabla_R | \Phi_j \rangle \frac{d\boldsymbol{R}}{dt}$$
$$= -i\hbar \langle \Phi_l | \frac{\partial}{\partial t} | \Phi_j \rangle \tag{13}$$

appears in eq 11 because the eigenfunctions of the electronic Hamiltonian, $\hat{H}(\mathbf{r}; \boldsymbol{R})$, which depends parametrically on atomic coordinates, also depend on atomic coordinates, $|\Phi_n(\mathbf{r}; \boldsymbol{R})\rangle$. Generally, d_{nj} promotes transitions between states n and j. The NA coupling reflects the dependence of the electronic wave functions on nuclear coordinates, and it is a form of electron−phonon coupling.

2.2.2. Global Flux Surface Hopping. GFSH[72−74] is a generalization of fewest switches SH[44] (FSSH), that is the most popular SH approach, to allow transitions between states that are not coupled directly, for instance, during super-exchange[72,74] and Auger-type many-particle processes.[19,85] The GFSH algorithm defines the probability of a transition from state n to another state j within the time interval dt as well as the criterion of whether a SH happens or not. Here, one considers the population change of states n during time step $[t, t + dt]$

$$\Delta\rho_{nn} = \rho_{nn}(t + dt) - \rho_{nn}(t) \tag{14}$$

and classify the states into two groups, group A undergoing population decrease and group B undergoing population increase. The total population is conserved; thus, the decrease of group A is equal to the increase of group B. If the current active state belongs to group A, the surface hopping probability from n in A to any state j in B should be proportional to the population increase of state j. The hopping probability from state n is proportional to the ratio of its population decrease to the total population reduction in group A, $\frac{\Delta\rho_{nn}}{\Sigma_{k\in A}\Delta\rho_{kk}}$. The increment in state j coming from state n becomes $\Delta\rho_{jj}\frac{\Delta\rho_{nn}}{\Sigma_{k\in A}\Delta\rho_{kk}}$. Adding the normalization ρ_{nn}, one obtains the hopping probability

$$g_{nj} = \frac{1}{\rho_{nn}}\Delta\rho_{jj}\frac{\Delta\rho_{nn}}{\Sigma_{k\in A}\Delta\rho_{kk}} \tag{15}$$

Dividing g_{nj} by Δt gives the rate constant for transition from state n to state j. The rate constant evolves in time and is determined by solution of the quantum dynamics eq 9.

SH is a Monte Carlo type algorithm, in which the transition probability, eq 15, is used to sample stochastic realizations of the electron−nuclear dynamics. A uniform random number $\xi \in (0,1)$ is generated each time step and compared to the SH probabilities for all transitions from state n to all other states j from group B. The criterion

$$\sum_{k=1}^{k=j-1} g_{nj} < \xi < \sum_{k=1}^{k=j} g_{nj} \tag{16}$$

determines whether a particular transition takes place. Note that for a sufficiently small time step, the sum of the probabilities of all transitions from state n is less than 1.

SH modeling of electron−nuclear dynamics of many materials allow for the classical path approximation (CPA), which assumes that nuclear dynamics is weakly dependent on the electronic evolution, while the electronic dynamics remain driven by the nuclear dynamics. The situation arises, for instance, when thermal fluctuations of nuclei are larger in amplitude than differences in the nuclear geometries associated with different electronic states. CPA allows one to employ a ground state MD trajectory, compute the electronic Hamiltonian, eq 12, and the NA coupling, eq 13, along this trajectory, and sample initial nuclear geometries for the nonequilibrium quantum dynamics simulations from this trajectory as well. The CPA brings SH closer to master equations.

2.3. Connecting Surface Hopping to the Pauli Master Equation. The developed PME-GFSH method uses the GFSH transition probabilities, eq 15 to propagate the PME, eq 5. The rate, $\gamma_{n\to j}$ of transitions from a higher energy state n to a lower energy state j is obtained by dividing the GFSH transition probability g_{nj} by Δt. Any other SH probability, e.g., the FSSH probability,[44] can be used instead. Since the PME, eq 5, follows from the LME, eq 2, if states n and j are eigenstates of the electronic Hamiltonian, the PME-GFSH is a special case of the general class of LME-SH approaches, which can consider transitions between different kinds of electronic states, either eigenstates or not, and use different SH algorithms. The rate,$\gamma_{j\to n}$ of transitions upward in energy is obtained using the detailed balance conditions, eq 8

$$\gamma_{j\to n} = \gamma_{n\to j}\frac{e^{\beta(E_j-\mu)} + 1}{e^{\beta(E_n-\mu)} + 1} \tag{17}$$

Detailed balance for the Fermi−Dirac statistics is used here, because the focus is on ensemble of electrons. Boltzmann or Bose−Einstein statistics can be used instead, as needed.

The simulation also requires definition of initial conditions. The initial geometries of nuclei are samples from the appropriate classical ensemble, typically canonical or micro-canonical and occasionally isobaric−isothermal. The initial distribution of populations of electronic states corresponds to an experimental photoexcitation, or applied voltage, or another perturbation. Importantly, because the developed method evolves a distribution or particles, the electronic initial condition represents a nonequilibrium particle distribution, rather than a particular electronic state. Therefore, it is essential to evolve the density matrix, eq 9, rather than the wave function, in order to obtain the SH probabilities. Using the density matrix formulation of SH allows us to match the electronic initial conditions used in eqs 5 and 9, providing a consistent connection between the PME for the evolution of the particle distribution and the quantum Liouville−von Neumann equation for the evolution of the SH probabilities.

Note that in contrast to SH procedures, the current method requires no stochastic sampling, since the PME, eq 5, can be propagated deterministically.

3. APPLICATION: ELECTRON−PHONON RELAXATION IN METALLIC FILMS

In order to illustrate the utility of the LME-SH approach we consider electron−phonon relaxation in metallic films, representing the general interest in modeling scattering and relaxation of energy carriers for design of micro- and nanoscale devices.[86,87] We choose two well-studied systems, a Au

https://dx.doi.org/10.1021/acs.jpcb.0c03030
J. Phys. Chem. B 2020, 124, 4326−4337

film[7,82,88,89] and the Au film with a Ti adhesion.[84] The adhesion layer was introduced for synthesis purposes, to facilitate interaction between the film and a substrate. However, it was discovered unexpectedly that a narrow Ti adhesion layer drastically changed electron−phonon relaxation in the much thicker Au film.[72]

Traditionally, charge-phonon scattering in metallic systems was described by the phenomenological two temperature model[22,23] (TTM), according to which electrons and phonons exist as two reservoirs, each at their own temperature, and in which the two reservoirs exchange energy until the two temperatures become equal. The electron−phonon coupling constant of the TTM can be viewed as a heat capacity rate, having units that are more complex than just the energy units. Quantifying the volumetric rate of energy flow between the two reservoirs, the coupling constant typically comes from experiments. Zhigilei and co-workers[90] used electronic structure calculation to estimate the electron−phonon coupling constant in the TTM, and in particular, to consider its energy dependence arising from changes in the electronic density of states. Completely switching from the phenomenological TTM to the ab initio description, Zhou et al.[91−93] performed ab initio real-time TDDFT calculations combined with NAMD in order to model the nonequilibrium energy flow between photoexcited electrons and phonons, directly mimicking the time-resolved laser experiments.[7,86,88,89] While Zhou et al. propagated one photoexcited electron (or hole) at a time, we employ the same simulation setup in order to propagate the nonequilibrium distribution of electrons toward the Fermi−Dirac equilibrium in a single simulation, using the developed method.

3.1. Simulation Details. The simulations are performed with the PYXAID package[79,80] for quantum dynamics simulations. PYXAID builds on top of a DFT electronic structure code such as Quantum Espresso[94,95] (QE) and VASP, and it adds the real-time TDDFT/NAMD capability adapted for materials simulations. The GFSH algorithm[72] was already implemented in PYXAID, in particular, since it only requires changes of a few lines of the FSSH algorithm.[44] However, we had to implement propagation of the density matrix, eq 5, in place of the time-dependent Kohn−Sham equations, a type of Schrodinger equation, used in the original PYXAID.[79,80]

To simulate the experimentally studied Au films with and without a narrow Ti adhesion layer and to limit the computational cost with a reasonable cell size, we built an Au(111) surface with seven layers of Au atoms to simulate the gold film and added a layer of Ti atoms to model the Au film with a narrow Ti adhesion layer, as shown in Figure 1. The cell parameters of the pristine Au film, Figure 1a are $a = b = 5.76761$ and $c = 34.12769$ Å and $\alpha = 90$, $\beta = 90$, and $\gamma = 120$ deg. A vacuum layer of 20 Å is introduced into parameter c, the direction perpendicular to the surface, to avoid spurious interactions between periodic slabs. We construct the Au film with the Ti adhesion layer by place a Ti(001) layer with dimensions $a = b = 5.9012$ Å on the pristine Au(111) film surface, as shown in Figure 1c.

The geometry optimization and the electronic properties are obtained with QE[94,95] employing the Perdew−Burke−Ernzerhof[96] (PBE) functional and the projector-augmented wave (PAW) approach.[97] The Monkhorst−Pack mesh of 7 × 7 × 1 was used for the DOS calculations. The geometries of the Au films with and without the Ti adhesion layer were optimized at 0 K. Then, the systems were heated up to 300 K with Anderson thermalization. Following the thermalization, 3 ps microcanonical MD trajectories was obtained with a 1 fs time step. The adiabatic state energies and the NA couplings were calculated for each step of the MD runs. Thousand geometries were selected randomly from the adiabatic MD trajectories and were used as initial conditions for NA dynamics simulations. The initial conditions for the nonequilibrium distribution of electronic populations were set to mimic the 3.1 eV excitation energy in the pump−probe experiments by Giri et al.[7,98−100] Different distributions of the excitation energies between electrons and hole were considered. At time zero, the density matrix of eq 9 was diagonal, with the diagonal elements representing the initial populations of the electron and hole states.

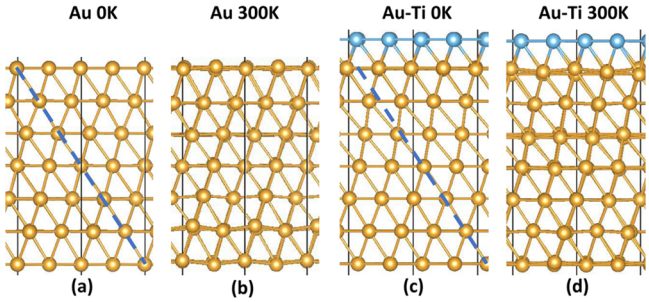

Figure 1. Optimized structures of the Au film with and without the Ti adhesion layer and representative structures at 300 K. Au is yellow and Ti is blue. The diagonal blue dashed line follows the perfect crystal structure of pristine Au and demonstrates distortion at the Au−Ti interface due to lattice mismatch.

3.2. Results and Discussion. Prior to discussing the quantum dynamics simulations, we briefly consider the geometric and electronic structure of the Au film with and without the Ti adhesion layer. The evolution of geometric properties changes energy gaps between electronic states and provides insights into the atomic motions contributing to the NA coupling, eq 13. Changes in the electronic density of states (DOS) due to Ti adhesion allow us to explain the differences in the relaxation dynamics of electrons and holes in the Au and Au/Ti systems.

3.2.1. Geometric and Electronic Structure. The optimized structures of the Au slab and the Au slab with the Ti adhesion layer, as well as representative structures at 300 K are shown in Figure 1. The optimized intralayer Au−Au bond lengths are 2.886 and 2.888 Å for the pristine Au and Au−Ti system, respectively, in good agreement with the experimental data.[100] The optimized Au−Ti bond length is 2.826 Å, which is also close to the experiments on Au−Ti bond lengths in clusters and alloys.[98] The Ti adhesion layer little influence on the Au−Au bond distance. However, Ti adhesion influences the top three Au layers by slightly shifting them laterally, as indicated by deviations from the dashed line in Figure 1c compared to Figure 1a. Heating induces fluctuations in the geometric structure in both systems, breaking the perfect crystal symmetry. Because Ti adhesion creates strain within the top Au layers, they are more susceptible to thermal fluctuations, as can be seen in Figure 1d. The notable influence of the Ti layer on the Au geometry indicates that the two metals interact strongly and that the enhanced motions at the interface can create significant NA coupling.

https://dx.doi.org/10.1021/acs.jpcb.0c03030
J. Phys. Chem. B 2020, 124, 4326−4337

Figures 2 and 3 show the density of state (DOS) of the Au and Au−Ti slabs in their optimized structures. The zero of

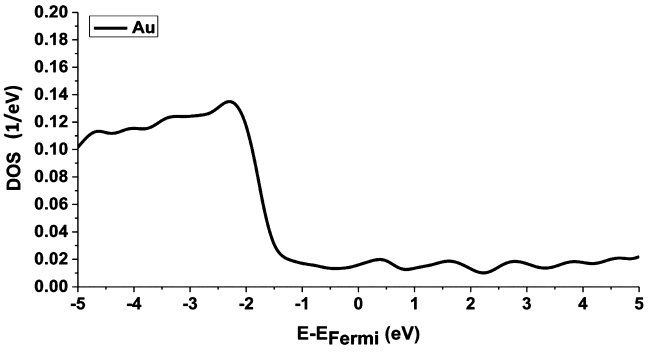

Figure 2. Density of states (DOS) of the pristine Au film. The Fermi energy is set as zero. The DOS is highly asymmetric with respect to the Fermi level, with the hole DOS much higher than the electron DOS.

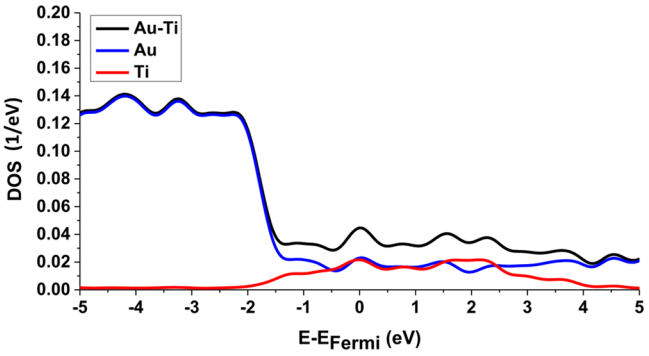

Figure 3. Partial and total densities of states (DOS) of the Au film with the Ti adhesion layer. The Fermi energy is set as zero. As the Au DOS drops between −2 and −1 eV, the Ti DOS rises. Note that the DOS of the 1-layer Ti is the same as the DOS of the 7-layer Au slab between −1 and +3 eV.

energy is set at the Fermi level. Since Au and Ti are metals, the systems have no bandgaps. The Au DOS is high at energies below −2 eV, due to contributions from Au d-electrons, and it undergoes a sharp drop in the energy range between −2 and −1 eV. Importantly, the contribution of Ti to the total DOS rises exactly where the Au partial DOS decreases in the Au−Ti system. The Ti partial DOS is negligible below −2 eV. However, at −1 eV and above, Au and Ti have nearly equal DOS, even though the number of Ti atoms in the Au−Ti slab is seven times smaller than the number of Au atoms. The strong contribution of the Ti atoms to the DOS in the −2 to 4 eV energy range arises from Ti d-electrons. The fact that the region of high Ti DOS matches the region of low Au DOS can rationalize the strong effect of the Ti adhesion layer on the electron−phonon dynamics in Au films, as seen experimentally.[95] Large DOS implies smaller gaps between electronic energy levels, resulting in larger NACs, because the NAC is inversely proportional to the energy gap, eq 13.

3.2.2. Quantum Dynamics of Electron Distribution. Modeling the 3.1 eV excitation energy used in the pump−probe experiments,[72] we consider the two asymmetric excitation limits, in which the energy is deposited primarily into either electrons, Figure 4, or holes, Figure 5. A symmetric excitation can be understood as the average of these two scenarios. Because the number of vacated levels below the Fermi energy should match the number of occupied levels above the Fermi energy, the lower DOS region constitutes the bottleneck. Therefore, most of the photoexcitation energy will be deposited to electrons, to sample a broader DOS range, and the hot electron/cold hole excitation scenario, Figure 4, is more likely than the opposite limit or a symmetric excitation.

Figures 4 and 5 show deviations of the electron distribution from the equilibrium Fermi−Dirac distribution at time 0 (left panels), and at later times. The upper panels describe the pristine Au system, while the lower panels correspond to the Au−Ti slab. Considering the hot electron/cold hole excitation, Figure 4, we observe a long electron relaxation time. By 80 fs in most of the holes in pristine Au have already relaxed to the Fermi level, while there still exists a notable populations of electrons at the initial energy. Even at 700 fs one can observe a small population of electrons far away from the Fermi energy. The situation is qualitatively similar in the Au−Ti system, however, the dynamics are significantly faster, in agreement with the experiment.[44] The charges have reached the equilibrium by 400 fs. Considering the cold electrons/hot holes scenario, one observes a faster dynamics, Figure 5. As in Figure 4, the holes equilibrate faster than the electrons, and the final stage of equilibration near the Fermi level is much faster in the presence of the Ti adhesion layer.

The differences in the electron and hole relaxation, and the strong influence of the Ti adhesion layer can be understood by considering the NA couplings, presented in Table 1 and defined in eq 13. According the first expression in eq 13, the NA coupling between a pair of states is inversely proportional to their energy difference and is proportional to nuclear velocity. Higher DOS leads to smaller energy differences, while nuclear velocities of light Ti atoms are much higher than velocities of heavy Au atoms. Therefore, the NA couplings are larger at energies below than above the Fermi level, due to the DOS asymmetry, Figures 2 and 3, and the couplings are enhanced strongly by light Ti atoms.

The quantum dynamics simulations of the phonon-induced relaxation of the nonequilibrium ensemble of electrons demonstrate the utility and efficiency of the developed approach. Compared to the previous simulation methodology[91−93] that considered one or few excited particles at a time, a single quantum dynamics trajectory of the current approach provides a complete picture by capturing evolution of the whole particle distribution. From the practical perspective, the results show that one can use a narrow adhesion layer to tune significantly electron−phonon dynamics in metallic slabs. The effect depends on the mass of atoms in the adhesion layer and its contribution of the total DOS. For example, one can selectively accelerate electron and hole relaxation or maintain the original properties of the Au film, by considering different stoichiometries of TiO_x adhesion layers.[101]

4. DISCUSSION AND CONCLUSIONS

Motivated by the need to model quantum dynamics of ensembles of electrons in metallic and semiconducting materials at the atomistic *ab initio* level of detail, we have developed, implemented and applied a novel approach combining the LME and SH. The master equation allows us to model efficiently evolution of particle ensembles that are hard to model at the fully quantum mechanical level using many-body wave functions or density matrices, due to

https://dx.doi.org/10.1021/acs.jpcb.0c03030
J. Phys. Chem. B 2020, 124, 4326−4337

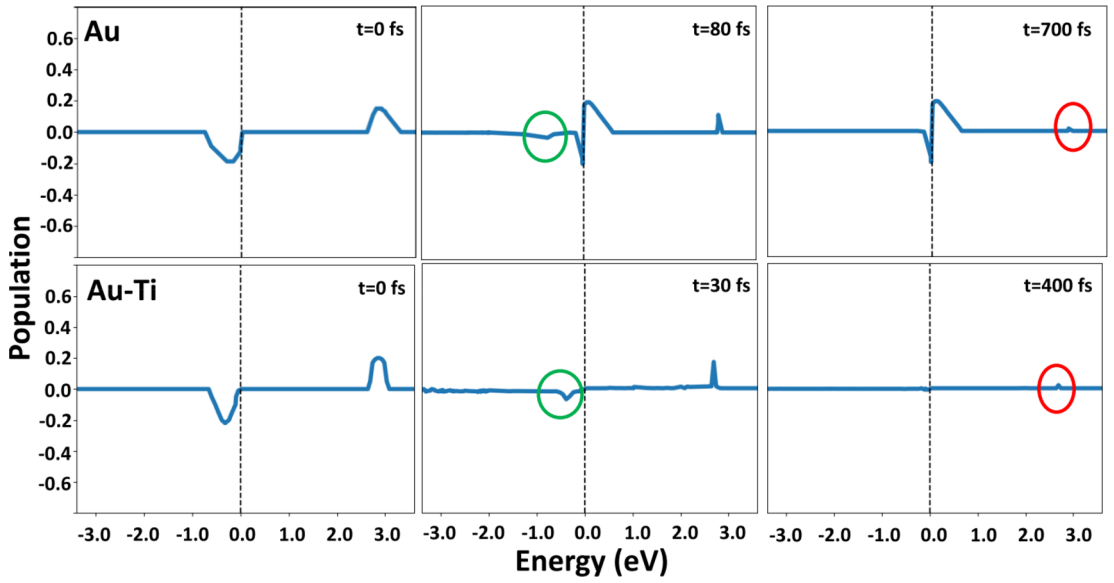

Figure 4. Deviation of the electron−hole distribution from the equilibrium Fermi−Dirac distribution at different times in the Au and Au−Ti systems. The initial distribution contains low energy holes and high energy electrons. The green circle highlights the last nonequilibrium hole snapshot, while the red circle highlights the last nonequilibrium electron snapshot. Hole relaxation are faster than electron relaxation in both systems, because the hole DOS is higher, Figures 2 and 3. Thus, the time to reach equilibrium is determined by electron relaxation. The charges relax faster in the Au−Ti system compared to pristine Au, because the NAC is larger, Table 1, due to presence of the lighter Ti atoms.

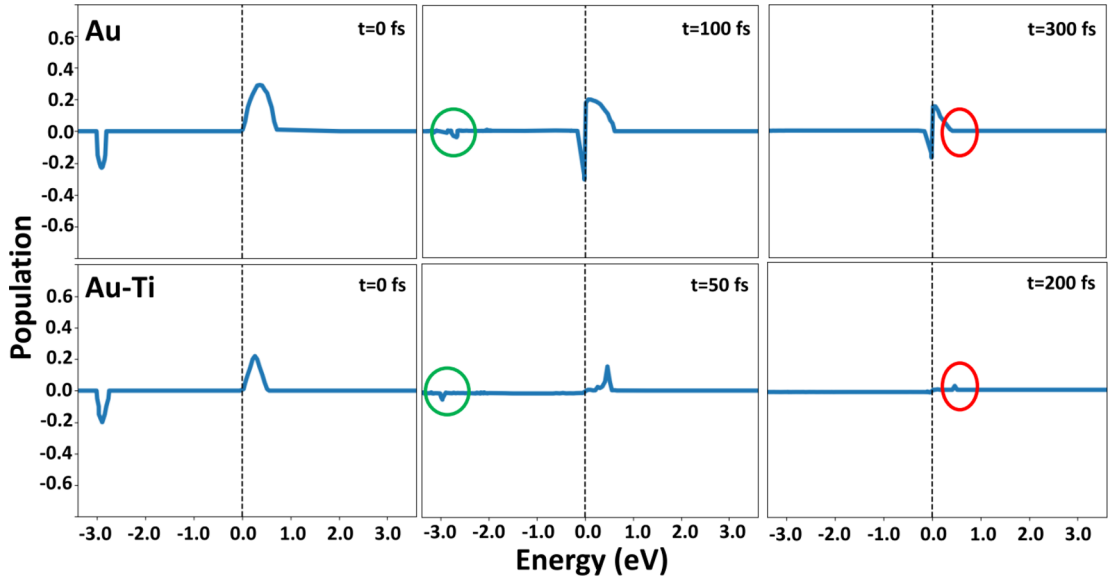

Figure 5. Deviation of the electron−hole distribution from the equilibrium Fermi−Dirac distribution at different times in the Au and Au−Ti systems. The initial distribution contains high energy holes and low energy electrons. The green circle highlights the last nonequilibrium hole snapshot, while the red circle highlights the last nonequilibrium electron snapshot. Because holes relax faster than electrons due to higher hole DOS, Figure 2, high energy holes and low energy electrons in pristine Au approach the Fermi energy on comparable time scales: 100 fs for holes and 300 fs for electrons. Compare with the opposite initial condition in Figure 4. The charges in the Au−Ti system reach equilibrium within 200 fs, because the Ti adhesion layer greatly accelerates the charge relaxation.

unfavorable exponential scaling with the number of particles. SH provides a nonperturbative atomistic description of transition rates that enter the LME. Traditionally, master equations employed perturbative expressions for transitions rates,[102] independent of time or instantaneous nuclear geometry, while SH was limited to few particle excitations. By viewing SH conceptually as a type of master equation rather than a generalization of classical MD and employing the density matrix rather than wave function formulation of SH, we bridged SH and traditional master equations and developed the new LME-SH technique.

We implemented the LME-SH method within *ab initio* real-time TDDFT using the PYXAID software package.[79,80] The implementation allows us to study a wide range of condensed phase and nanoscale materials, whose electronic structure can be described by DFT. In particular, we applied the method to investigate phonon-driven relaxation of electrons in metallic films. The simulations rationalized the strong dependence of electron−phonon relaxation in an Au film on the presence of a

https://dx.doi.org/10.1021/acs.jpcb.0c03030
J. Phys. Chem. B 2020, 124, 4326−4337

Table 1. Absolute NAC Averaged over States within Different Energy Ranges in the Au and Au−Ti Slabs at 300 K[a]

	NAC (meV)		
	−3 to 0 eV	−0.5 to +0.5 eV	0 to 3 eV
Au	1.26	1.43	1.10
Au−Ti	1.75	2.49	1.27

[a]The narrow Ti adhesion layer increases the NAC, in particular at energies near the Fermi level.

narrow Ti adhesion layer observed experimentally,[98] and they rationalized atomistically the mechanism underlying this phenomenon.

Performing simulations on a particle ensemble in a single simulation using a master equation is much more computationally efficient than solving the Schrodinger equation and obtaining one SH trajectory at a time. The advantage becomes particularly apparent if one considers solving the Schrodinger equation for a wave function representing excitation of tens of particles, as is common in metallic systems. The dimensionality of such simulation is enormous, making it essentially impossible. At the same time, obtaining transition rates from solution of a low-dimensional Schrodinger equation representing electron−vibrational or two particle electron−electron scattering can be achieved easily at the ab initio level. Therefore, the method is not much more difficult computationally than solution of a master equation with Fermi golden rule type transition rates.[102]

Compared to master equations with perturbative transition rates, evaluation of SH transition rates captures dependence of electronic properties on atomic evolution, and includes explicit electron−nuclear correlations. Vibrations are treated by *ab initio* MD, and therefore, atoms are not restricted to vibrate only around their equilibrium positions. The LME-SH method can be used to model electron−nuclear dynamics of liquid metals, for example, or to follow photoinduced structural phase transitions induced by excitations of ensembles of electrons.[38−40] Because of a large number of excited electrons, such processes cannot be modeled by traditional SH due to exponential scaling of dimensionality of the full quantum dynamics of the electronic subsystem.

Master equations provide reduced descriptions, compared to solution of the full quantum mechanical problem, as given by the Schrodinger equation. The LME-SH method solves a reduced dimensional Schrodinger equation and uses it as input to the master equation. In the current implementation, the Schrodinger equation is solved for a single excited electron, representing electron-vibrational interactions. Typically, electron−electron scattering happens faster than electron−phonon scattering, and therefore, one can focus on one type of interaction at a time. However, there exist cases, in which charge−charge and charge−phonon scattering occur on similar time scales.[19,56,85,103,104] One can extend beyond the single particle description and develop master equations for two, three, or four particle states describing excitons, trions, double excitons, etc. Even though charge−charge scattering occurs in large ensembles of particles, elementary processes are few-body, allowing one to employ reduced representations. Electron−phonon coupling can vary strongly with time, because phonons can be highly anharmonic in complex materials, and energies and wave functions of electronic levels can depend strongly on nuclear geometry. Similarly, electron−electron scattering can change significantly along a nuclear trajectory. The use of SH transition rates allows one to include geometry and time dependence of electron−phonon and electron−electron scattering explicitly and at the *ab initio* level.

As a next step, one can consider two-particle excitations in the presence of vibrational motions, solve the corresponding Schrodinger equation, and compute SH transition rates that include both electron−electron (or electron−hole) and electron−vibrational energy exchange. Such models can describe Auger-assisted charge transfer[15,104] and trapping[19,85,103] by defect states, in which the particle of interest can exchange energy with both the other particle and vibrations. Including 3- and 4-particle excitations can allow one to model Auger-assisted electron−hole recombination and multiple exciton generation and annihilation.[5,9,10,12,13,24,56] Considering 4-particle excitations even in small clusters is already very expensive at the level of the Schrodinger equation, requiring solving quantum dynamics in the basis of hundreds of thousands of states.[56] The scaling is similar to configuration interaction in the electronic structure theory. The LME-SH technique allows one to consider the most important, few particle processes at a nonperturbative level, while modeling evolution of large ensembles of particles.

The current implementation of the LME-SH method uses the CPA, which is applicable to many nanoscale and bulk materials, and which creates significant computational savings. The CPA allows one to model nonequilibrium dynamics of the quantum (electronic) subsystem using a predetermined trajectory for the classical (atomic) degrees of freedom. In *ab initio* NAMD, one can use a ground state trajectory and avoid the need to calculate excited state potential energy surfaces, which constitutes a challenging task. The LME-SH approach does not require the CPA. Because atomic evolution is coupled to evolution of an electron ensemble, the method becomes similar to the mean-field/Ehrenfest approach in the absence of CPA, because atoms feel the average force of electrons. The Ehrenfest approach is known to disobey detailed balance between transitions upward and downward in energy, required to achieve thermodynamic equilibrium. Currently, the detailed balance is enforced by eq 17, which is used in combination with the CPA. If the CPA is not invoked, the detailed balance can be achieved similarly to the Ehrenfest approach by introducing nonlinear terms in the electronic NA Hamiltonian[31,105] and related ideas.[106]

Loss of coherence within the electronic subsystem induced by nuclei can play important roles in condensed phase simulations.[50,107−111] Decoherence effects are missing if nuclei are treated by classical MD in a straightforward way. While decoherence corrections are not required in modeling quantum dynamics occurring within dense manifolds of states, as in the metallic films simulated here, they become essential for transitions across significant energy gaps. The LME provides a natural framework to include decoherence through the nonunitary terms of eq 2. Decoherence corrections can be introduced as in the Ehrenfest method,[107,112−115] and both decoherence and detailed balance effects can be introduced simultaneously.[31,112,114]

The LME reduces to the PME in the adiabatic representation. Similar to SH, simulations can be carried out in the diabatic representation as well, in which the electronic Hamiltonian is not diagonal. For example, by using the single particle basis and adding electron−hole interactions as off-diagonal terms into the Hamiltonian, one can capture excitonic

https://dx.doi.org/10.1021/acs.jpcb.0c03030
J. Phys. Chem. B 2020, 124, 4326−4337

effects. However, in order to represent electron−hole scattering, one needs to introduce corresponding scattering rates into the nonunitary terms of the master equations. Such rates can be obtained using SH expressions as well. Thus, the approach allows one to consider both coherent electron−phonon and electron−electron interactions, and incoherent charge-phonon and charge−charge scattering processes. The LME-SH technique developed and implemented in this work provides a general framework for studying efficiently and realistically quantum dynamics in a broad range of complex condensed matter systems.

AUTHOR INFORMATION

Corresponding Author

Oleg V. Prezhdo − *Department of Chemistry and Department of Physics and Astronomy, University of Southern California, Los Angeles, California 90089, United States;* orcid.org/0000-0002-5140-7500; Email: : prezhdo@usc.edu

Authors

Yi-Siang Wang − *Department of Chemistry, University of Southern California, Los Angeles, California 90089, United States*

Parmeet Nijjar − *Department of Chemistry, University of Southern California, Los Angeles, California 90089, United States*

Xin Zhou − *Department of Chemistry, University of Southern California, Los Angeles, California 90089, United States; College of Environment and Chemical Engineering, Dalian University, Dalian 116622, P. R. China;* orcid.org/0000-0002-4385-8379

Denys I. Bondar − *Department of Physics and Engineering Physics, Tulane University, New Orleans, Louisiana 70118, United States*

Complete contact information is available at: https://pubs.acs.org/10.1021/acs.jpcb.0c03030

Notes

The authors declare no competing financial interest.

ACKNOWLEDGMENTS

Y.-S.W., P.N., and O.V.P. acknowledge financial support from the US National Science Foundation (Grant No. CHE-1900510), for the methods development, and from the US Department of Defense, Multidisciplinary University Research Initiative (Grant No. W911NF-16-1-0406), for the applications. D.I.B. is supported by Air Force Office of Scientific Research (AFOSR) Young Investigator Research Program (Grant FA9550-16-1-0254) and the Army Research Office (ARO) (Grant W911NF-19-1-0377). The views and conclusions contained in this document are those of the authors and should not be interpreted as representing the official policies, either expressed or implied, of AFOSR, ARO, or the U.S. Government. The U.S. Government is authorized to reproduce and distribute reprints for Government purposes notwithstanding any copyright notation herein.

REFERENCES

(1) Jailaubekov, A. E.; et al. Hot Charge-Transfer Excitons Set the Time Limit for Charge Separation at Donor/Acceptor Interfaces in Organic Photovoltaics. *Nat. Mater.* **2013**, *12*, 66−73.

(2) Rossky, P. J.; Schnitker, J. The Hydrated Electron - Quantum Simulation of Structure, Spectroscopy and Dynamics. *J. Phys. Chem.* **1988**, *92*, 4277−4285.

(3) Wong, K. F.; Bagchi, B.; Rossky, P. J. Distance and Orientation Dependence of Excitation Transfer Rates in Conjugated Systems: Beyond the Forster Theory. *J. Phys. Chem. A* **2004**, *108*, 5752−5763.

(4) Worley, B. C.; Haws, R. T.; Rossky, P. J.; Dodabalapur, A. Chemical Understanding of the Mechanisms Involved in Mitigation of Charged Impurity Effects by Polar Molecules on Graphene. *J. Phys. Chem. C* **2016**, *120*, 12909−12916.

(5) Beard, M. C.; Johnson, J. C.; Luther, J. M.; Nozik, A. J. Multiple Exciton Generation in Quantum Dots Versus Singlet Fission in Molecular Chromophores for Solar Photon Conversion. *Philos. Trans. R. Soc., A* **2015**, *373*, 20140412.

(6) Bharadwaj, P.; Bouhelier, A.; Novotny, L. Electrical Excitation of Surface Plasmons. *Phys. Rev. Lett.* **2011**, *106*, 226802.

(7) Giri, A.; Hopkins, P. E. Transient Thermal and Nonthermal Electron and Phonon Relaxation after Short-Pulsed Laser Heating of Metals. *J. Appl. Phys.* **2015**, *118*, 215101.

(8) Kelly, K. L.; Coronado, E.; Zhao, L. L.; Schatz, G. C. The Optical Properties of Metal Nanoparticles: The Influence of Size, Shape, and Dielectric Environment. *J. Phys. Chem. B* **2003**, *107*, 668−677.

(9) Klimov, V. I. Mechanisms for Photogeneration and Recombination of Multiexcitons in Semiconductor Nanocrystals: Implications for Lasing and Solar Energy Conversion. *J. Phys. Chem. B* **2006**, *110*, 16827−16845.

(10) Prezhdo, O. V. Multiple Excitons and the Electron-Phonon Bottleneck in Semiconductor Quantum Dots: An Ab Initio Perspective. *Chem. Phys. Lett.* **2008**, *460*, 1−9.

(11) Sprague-Klein, E. A.; McAnally, M. O.; Zhdanov, D. V.; Zrimsek, A. B.; Apkarian, V. A.; Seideman, T.; Schatz, G. C.; Van Duyne, R. P. Observation of Single Molecule Plasmon-Driven Electron Transfer in Isotopically Edited 4,4'-Bipyridine Gold Nanosphere Oligomers. *J. Am. Chem. Soc.* **2017**, *139*, 15212−15221.

(12) Wang, S.; Khafizov, M.; Tu, X.; Zheng, M.; Krauss, T. D. Multiple Exciton Generation in Single-Walled Carbon Nanotubes. *Nano Lett.* **2010**, *10*, 2381−6.

(13) Yang, Y.; Rodríguez-Córdoba, W.; Lian, T. Multiple Exciton Generation and Dissociation in Pbs Quantum Dot-Electron Acceptor Complexes. *Nano Lett.* **2012**, *12*, 4235−4241.

(14) Zhang, Z. S.; Liu, L. H.; Fang, W. H.; Long, R.; Tokina, M. V.; Prezhdo, O. V. Plasmon-Mediated Electron Injection from Au Nanorods into Mos2: Traditional Versus Photoexcitation Mechanism. *Chem.* **2018**, *4*, 1112−1127.

(15) Zhu, H. M.; Yang, Y.; Hyeon-Deuk, K.; Califano, M.; Song, N. H.; Wang, Y. W.; Zhang, W. Q.; Prezhdo, O. V.; Lian, T. Q. Auger-Assisted Electron Transfer from Photoexcited Semiconductor Quantum Dots. *Nano Lett.* **2014**, *14*, 1263−1269.

(16) Zhu, X. Y.; Podzorov, V. Charge Carriers in Hybrid Organic-Inorganic Lead Halide Perovskites Might Be Protected as Large Polarons. *J. Phys. Chem. Lett.* **2015**, *6*, 4758−61.

(17) Castro Neto, A. H.; Guinea, F.; Peres, N. M. R.; Novoselov, K. S.; Geim, A. K. The Electronic Properties of Graphene. *Rev. Mod. Phys.* **2009**, *81*, 109−162.

(18) Ferguson, B.; Zhang, X. C. Materials for Terahertz Science and Technology. *Nat. Mater.* **2002**, *1*, 26−33.

(19) Li, L. Q.; et al. Phonon-Suppressed Auger Scattering of Charge Carriers in Defective Two-Dimensional Transition Metal Dichalcogenides. *Nano Lett.* **2019**, *19*, 6078−6086.

(20) Leijtens, T.; Eperon, G. E.; Barker, A. J.; Grancini, G.; Zhang, W.; Ball, J. M.; Kandada, A. R. S.; Snaith, H. J.; Petrozza, A. Carrier Trapping and Recombination: The Role of Defect Physics in Enhancing the Open Circuit Voltage of Metal Halide Perovskite Solar Cells. *Energy Environ. Sci.* **2016**, *9*, 3472−3481.

(21) Li, W.; Long, R.; Tang, J. F.; Prezhdo, O. V. Influence of Defects on Excited-State Dynamics in Lead Halide Perovskites: Time-Domain Ab Initio Studies. *J. Phys. Chem. Lett.* **2019**, *10*, 3788−3804.

(22) Anisimov, S. I.; Kapeliovich, B. L.; Perelman, T. L. Electron Emission from Metal Surfaces Exposed to Ultrashort Laser Pulses. *Zh. Eksp. Teor. Fiz.* **1974**, *66*, 375−377.
(23) Qiu, T. Q.; Tien, C. L. Heat Transfer Mechanisms During Short-Pulse Laser Heating of Metals. *J. Heat Transfer* **1993**, *115*, 835−841.
(24) Tsai, C. Y. The Effects of Intraband and Interband Carrier-Carrier Scattering on Hot-Carrier Solar Cells: A Theoretical Study of Spectral Hole Burning, Electron-Hole Energy Transfer, Auger Recombination, and Impact Ionization Generation. *Prog. Photovoltaics* **2019**, *27*, 433−452.
(25) Vollbrecht, J.; Brus, V. V.; Ko, S. J.; Lee, J.; Karki, A.; Cao, D. X.; Cho, K.; Bazan, G. C.; Nguyen, T. Q. Quantifying the Nongeminate Recombination Dynamics in Nonfullerene Bulk Heterojunction Organic Solar Cells. *Adv. Energy Mater.* **2019**, *9*, 1901438.
(26) Toyoura, K.; Fujii, T.; Hatada, N.; Han, D.; Uda, T. Carrier−Carrier Interaction in Proton-Conducting Perovskites: Carrier Blocking Vs Trap-Site Filling. *J. Phys. Chem. C* **2019**, *123*, 26823−26830.
(27) Marques, M. A.; Gross, E. K. Time-Dependent Density Functional Theory. *Annu. Rev. Phys. Chem.* **2004**, *55*, 427−55.
(28) Tully, J. C. Mixed Quantum−Classical Dynamics. *Faraday Discuss.* **1998**, *110*, 407−419.
(29) Andrade, X.; et al. Time-Dependent Density-Functional Theory in Massively Parallel Computer Architectures: The Octopus Project. *J. Phys.: Condens. Matter* **2012**, *24*, 233202.
(30) Li, X. S.; Tully, J. C.; Schlegel, H. B.; Frisch, M. J. Ab Initio Ehrenfest Dynamics. *J. Chem. Phys.* **2005**, *123*, No. 084106.
(31) Nijjar, P.; Jankowska, J.; Prezhdo, O. V. Ehrenfest and Classical Path Dynamics with Decoherence and Detailed Balance. *J. Chem. Phys.* **2019**, *150*, 204124.
(32) Parandekar, P. V.; Tully, J. C. Detailed Balance in Ehrenfest Mixed Quantum-Classical Dynamics. *J. Chem. Theory Comput.* **2006**, *2*, 229−235.
(33) Tempel, D. G.; Aspuru-Guzik, A. Relaxation and Dephasing in Open Quantum Systems Time-Dependent Density Functional Theory: Properties of Exact Functionals from an Exactly-Solvable Model System. *Chem. Phys.* **2011**, *391*, 130−142.
(34) Xue, Y. Q.; Datta, S.; Ratner, M. A. First-Principles Based Matrix Green's Function Approach to Molecular Electronic Devices: General Formalism. *Chem. Phys.* **2002**, *281*, 151−170.
(35) Redfield, A. G. The Theory of Relaxation Processes. *Adv. Magn. Opt. Reson.* **1965**, *1*, 1−32.
(36) Marronnier, A.; Lee, H.; Geffroy, B.; Even, J.; Bonnassieux, Y.; Roma, G. Structural Instabilities Related to Highly Anharmonic Phonons in Halide Perovskites. *J. Phys. Chem. Lett.* **2017**, *8*, 2659−2665.
(37) Li, W.; Vasenko, A. S.; Tang, J. F.; Prezhdo, O. V. Anharmonicity Extends Carrier Lifetimes in Lead Halide Perovskites at Elevated Temperatures. *J. Phys. Chem. Lett.* **2019**, *10*, 6219−6226.
(38) Bisoyi, H. K.; Li, Q. Light-Driven Liquid Crystalline Materials: From Photo-Induced Phase Transitions and Property Modulations to Applications. *Chem. Rev.* **2016**, *116*, 15089−15166.
(39) Cavalleri, A.; Toth, C.; Siders, C. W.; Squier, J. A.; Raksi, F.; Forget, P.; Kieffer, J. C. Femtosecond Structural Dynamics in Vo2 During an Ultrafast Solid-Solid Phase Transition. *Phys. Rev. Lett.* **2001**, *87*, 237401.
(40) Lin, Y. C.; Dumcenco, D. O.; Huang, Y. S.; Suenaga, K. Atomic Mechanism of the Semiconducting-to-Metallic Phase Transition in Single-Layered Mos2. *Nat. Nanotechnol.* **2014**, *9*, 391−396.
(41) Lindblad, G. On the Generators of Quantum Dynamical Semigroups. *Commun. Math. Phys.* **1976**, *48*, 119−130.
(42) Choi, M.-D. Completely Positive Linear Maps on Complex Matrices. *Linear Algebra and its Applications* **1975**, *10*, 285−290.
(43) Herman, M. F. Nonadiabatic Semiclassical Scattering. I. Analysis of Generalized Surface Hopping Procedures. *J. Chem. Phys.* **1984**, *81*, 754−763.
(44) Tully, J. C. Molecular Dynamics with Electronic Transitions. *J. Chem. Phys.* **1990**, *93*, 1061−1071.
(45) Webster, F.; Rossky, P. J.; Friesner, R. A. Nonadiabatic Processes in Condensed Matter - Semiclassical Theory and Implementation. *Comput. Phys. Commun.* **1991**, *63*, 494−522.
(46) Wang, L. J.; Akimov, A.; Prezhdo, O. V. Recent Progress in Surface Hopping: 2011−2015. *J. Phys. Chem. Lett.* **2016**, *7*, 2100−2112.
(47) Barbatti, M. Nonadiabatic Dynamics with Trajectory Surface Hopping Method. *Wiley Interdisciplinary Reviews-Computational Molecular Science* **2011**, *1*, 620−633.
(48) Hack, M. D.; Truhlar, D. G. Nonadiabatic Trajectories at an Exhibition. *J. Phys. Chem. A* **2000**, *104*, 7917−7926.
(49) Subotnik, J. E.; Jain, A.; Landry, B.; Petit, A.; Ouyang, W. J.; Bellonzi, N. Understanding the Surface Hopping View of Electronic Transitions and Decoherence. *Annu. Rev. Phys. Chem.* **2016**, *67*, 387−417.
(50) Bittner, E. R.; Rossky, P. J. Quantum Decoherence in Mixed Quantum-Classical Systems - Nonadiabatic Processes. *J. Chem. Phys.* **1995**, *103*, 8130−8143.
(51) Prezhdo, O. V.; Rossky, P. J. Mean-Field Molecular Dynamics with Surface Hopping. *J. Chem. Phys.* **1997**, *107*, 825−834.
(52) Craig, C. F.; Duncan, W. R.; Prezhdo, O. V. Trajectory Surface Hopping in the Time-Dependent Kohn-Sham Approach for Electron-Nuclear Dynamics. *Phys. Rev. Lett.* **2005**, *95*, 163001.
(53) Fischer, S. A.; Habenicht, B. F.; Madrid, A. B.; Duncan, W. R.; Prezhdo, O. V. Regarding the Validity of the Time-Dependent Kohn-Sham Approach for Electron-Nuclear Dynamics Via Trajectory Surface Hopping. *J. Chem. Phys.* **2011**, *134*, No. 024102.
(54) Doltsinis, N. L.; Marx, D. Nonadiabatic Car-Parrinello Molecular Dynamics. *Phys. Rev. Lett.* **2002**, *88*, 166402.
(55) Tapavicza, E.; Tavernelli, I.; Rothlisberger, U. Trajectory Surface Hopping within Linear Response Time-Dependent Density-Functional Theory. *Phys. Rev. Lett.* **2007**, *98*, No. 023001.
(56) Hyeon-Deuk, K.; Prezhdo, O. V. Multiple Exciton Generation and Recombination Dynamics in Small Si and Cdse Quantum Dots: An Ab Initio Time-Domain Study. *ACS Nano* **2012**, *6*, 1239−1250.
(57) Sakhavand, N.; Shahsavari, R. Dimensional Crossover of Thermal Transport in Hybrid Boron Nitride Nanostructures. *ACS Appl. Mater. Interfaces* **2015**, *7*, 18312−18319.
(58) Lu, Z.; Wang, Y.; Ruan, X. Metal/Dielectric Thermal Interfacial Transport Considering Cross-Interface Electron-Phonon Coupling: Theory, Two-Temperature Molecular Dynamics, and Thermal Circuit. *Phys. Rev. B: Condens. Matter Mater. Phys.* **2016**, *93*, No. 064302.
(59) Wang, G.; Feng, H.; Gao, A.; Hao, Q.; Jin, W.; Peng, X.; Li, W.; Wu, G.; Chu, P. K. Extracellular Electron Transfer from Aerobic Bacteria to Au-Loaded Tio2 Semiconductor without Light: A New Bacteria-Killing Mechanism Other Than Localized Surface Plasmon Resonance or Microbial Fuel Cells. *ACS Appl. Mater. Interfaces* **2016**, *8*, 24509−16.
(60) Luo, T.; Chen, G. Nanoscale Heat Transfer - from Computation to Experiment. *Phys. Chem. Chem. Phys.* **2013**, *15*, 3389−3412.
(61) Pop, E. Energy Dissipation and Transport in Nanoscale Devices. *Nano Res.* **2010**, *3*, 147−169.
(62) Zheng, K.; Sun, F. Y.; Tian, X.; Zhu, J.; Ma, Y. M.; Tang, D. W.; Wang, F. S. Tuning the Interfacial Thermal Conductance between Polystyrene and Sapphire by Controlling the Interfacial Adhesion. *ACS Appl. Mater. Interfaces* **2015**, *7*, 23644−23649.
(63) Allen, P. B. Theory of Thermal Relaxation of Electrons in Metals. *Phys. Rev. Lett.* **1987**, *59*, 1460−1463.
(64) Cahill, D. G.; Ford, W. K.; Goodson, K. E.; Mahan, G. D.; Majumdar, A.; Maris, H. J.; Merlin, R.; Phillpot, S. R. Nanoscale Thermal Transport. *J. Appl. Phys.* **2003**, *93*, 793−818.
(65) Lee, E.; Zhang, T.; Yoo, T. H.; Guo, Z.; Luo, T. F. Nanostructures Significantly Enhance Thermal Transport across Solid Interfaces. *ACS Appl. Mater. Interfaces* **2016**, *8*, 35505−35512.

https://dx.doi.org/10.1021/acs.jpcb.0c03030
J. Phys. Chem. B 2020, 124, 4326−4337

(66) Zhang, T.; Gans-Forrest, A. R.; Lee, E.; Zhang, X. Q.; Qu, C.; Pang, Y. S.; Sun, F.; Luo, T. F. Role of Hydrogen Bonds in Thermal Transport across Hard/Soft Material Interfaces. *ACS Appl. Mater. Interfaces* **2016**, *8*, 33326−33334.
(67) Wang, W.; Cahill, D. G. Limits to Thermal Transport in Nanoscale Metal Bilayers Due to Weak Electron-Phonon Coupling in Au and Cu. *Phys. Rev. Lett.* **2012**, *109*, 175503.
(68) Hopkins, P. E.; Phinney, L. M.; Serrano, J. R. Re-Examining Electron-Fermi Relaxation in Gold Films with a Nonlinear Thermoreflectance Model. *J. Heat Transfer* **2011**, *133*, 044505.
(69) Giri, A.; Gaskins, J. T.; Donovan, B. F.; Szwejkowski, C.; Warzoha, R. J.; Rodriguez, M. A.; Ihlefeld, J.; Hopkins, P. E. Mechanisms of Nonequilibrium Electron-Phonon Coupling and Thermal Conductance at Interfaces. *J. Appl. Phys.* **2015**, *117*, 105105.
(70) Varghese, R.; Harikrishna, H.; Huxtable, S. T.; Reynolds, W. T.; Priya, S. Effect of Crystallinity on Thermal Transport in Textured Lead Zirconate Titanate Thin Films. *ACS Appl. Mater. Interfaces* **2014**, *6*, 6748−6756.
(71) Eesley, G. L. Observation of Nonequilibrium Electron Heating in Copper. *Phys. Rev. Lett.* **1983**, *51*, 2140−2143.
(72) Wang, L.; Trivedi, D.; Prezhdo, O. V. Global Flux Surface Hopping Approach for Mixed Quantum-Classical Dynamics. *J. Chem. Theory Comput.* **2014**, *10*, 3598−3605.
(73) Sifain, A. E.; Wang, L. J.; Prezhdo, O. V. Mixed Quantum-Classical Equilibrium in Global Flux Surface Hopping. *J. Chem. Phys.* **2015**, *142*, 224102.
(74) Wang, L. J.; Sifain, A. E.; Prezhdo, O. V. Communication: Global Flux Surface Hopping in Liouville Space. *J. Chem. Phys.* **2015**, *143*, 191102.
(75) Tong, C. J.; Li, L. Q.; Liu, L. M.; Prezhdo, O. V. Synergy between Ion Migration and Charge Carrier Recombination in Metal-Halide Perovskites. *J. Am. Chem. Soc.* **2020**, *142*, 3060−3068.
(76) Alicki, R.; Lendi, K. *Quantum Dynamical Semigroups and Applications*; Springer Berlin: Berlin, 2014.
(77) Carmichael, H. *An Open Systems Approach to Quantum Optics: Lectures Presented at the Université Libre De Bruxelles, October 28 to November 4, 1991*; Springer Berlin: Berlin, 2014.
(78) Alicki, R. On the Detailed Balance Condition for Non-Hamiltonian Systems. *Rep. Math. Phys.* **1976**, *10*, 249−258.
(79) Akimov, A. V.; Prezhdo, O. V. The Pyxaid Program for Non-Adiabatic Molecular Dynamics in Condensed Matter Systems. *J. Chem. Theory Comput.* **2013**, *9*, 4959−72.
(80) Akimov, A. V.; Prezhdo, O. V. Advanced Capabilities of the Pyxaid Program: Integration Schemes, Decoherence Effects, Multi-excitonic States, and Field-Matter Interaction. *J. Chem. Theory Comput.* **2014**, *10*, 789−804.
(81) Wittig, C. The Landau− Zener Formula. *J. Phys. Chem. B* **2005**, *109*, 8428−8430.
(82) Alijah, A.; Nikitin, E. E. Fast Quantum, Semiclassical and Classical Dynamics near the Conical Intersection. *Mol. Phys.* **1999**, *96*, 1399−1410.
(83) Miller, W. H.; George, T. F. Semiclassical Theory of Electronic Transitions in Low-Energy Atomic and Molecular Collisions Involving Several Nuclear Degrees of Freedom. *J. Chem. Phys.* **1972**, *56*, 5637.
(84) Zhu, C.; Teranishi, Y.; Nakamura, H. Nonadiabatic Transitions Due to Curve Crossings: Complete Solutions of the Landau-Zener-Stueckelberg Problems and Their Applications. *Advances in Chemical Physics* **2007**, *117*, 127−233.
(85) Trivedi, D. J.; Wang, L. J.; Prezhdo, O. V. Auger-Mediated Electron Relaxation Is Robust to Deep Hole Traps: Time-Domain Ab Initio Study of Cdse Quantum Dots. *Nano Lett.* **2015**, *15*, 2086−2091.
(86) Rowlette, J. A.; Goodson, K. E. Fully Coupled Nonequilibrium Electron−Phonon Transport in Nanometer-Scale Silicon Fets. *IEEE Trans. Electron Devices* **2008**, *55*, 220−232.
(87) Robertson, J. High Dielectric Constant Gate Oxides for Metal Oxide Si Transistors. *Rep. Prog. Phys.* **2006**, *69*, 327−396.
(88) Hopkins, P. E.; Kassebaum, J. L.; Norris, P. M. Effects of Electron Scattering at Metal-Nonmetal Interfaces on Electron-Phonon Equilibration in Gold Films. *J. Appl. Phys.* **2009**, *105*, No. 023710.
(89) Radue, E. L.; Tomko, J. A.; Giri, A.; Braun, J. L.; Zhou, X.; Prezhdo, O. V.; Runnerstrom, E. L.; Maria, J. P.; Hopkins, P. E. Hot Electron Thermoreflectance Coefficient of Gold During Electron-Phonon Nonequilibrium. *ACS Photonics* **2018**, *5*, 4880−4887.
(90) Conwell, E. M.; McLaughlin, P. M.; Bloch, S. M. Charge-Transfer Excitons in DNA. *J. Phys. Chem. B* **2008**, *112*, 2268−2272.
(91) Zhou, X.; Jankowska, J.; Li, L.; Giri, A.; Hopkins, P. E.; Prezhdo, O. V. Strong Influence of Ti Adhesion Layer on Electron-Phonon Relaxation in Thin Gold Films: Ab Initio Nonadiabatic Molecular Dynamics. *ACS Appl. Mater. Interfaces* **2017**, *9*, 43343−43351.
(92) Wang, Y. S.; Zhou, X.; Tomko, J. A.; Giri, A.; Hopkins, P. E.; Prezhdo, O. V. Electron-Phonon Relaxation at Au/Ti Interfaces Is Robust to Alloying: Ab Initio Nonadiabatic Molecular Dynamics. *J. Phys. Chem. C* **2019**, *123*, 22842−22850.
(93) Zhou, X.; Tokina, M. V.; Tomko, J. A.; Braun, J. L.; Hopkins, P. E.; Prezhdo, O. V. Thin Ti Adhesion Layer Breaks Bottleneck to Hot Hole Relaxation in Au Films. *J. Chem. Phys.* **2019**, *150*, 184701.
(94) Giannozzi, P.; et al. Quantum Espresso: A Modular and Open-Source Software Project for Quantum Simulations of Materials. *J. Phys.: Condens. Matter* **2009**, *21*, 395502.
(95) Giannozzi, P.; et al. Advanced Capabilities for Materials Modelling with Quantum Espresso. *J. Phys.: Condens. Matter* **2017**, *29*, 465901.
(96) Perdew, J. P.; Burke, K.; Ernzerhof, M. Generalized Gradient Approximation Made Simple [Phys. Rev. Lett. 77, 3865 (1996)]. *Phys. Rev. Lett.* **1997**, *78*, 1396−1396.
(97) Blöchl, P. E. Projector Augmented-Wave Method. *Phys. Rev. B: Condens. Matter Mater. Phys.* **1994**, *50*, 17953−17979.
(98) Svanidze, E.; et al. High Hardness in the Biocompatible Intermetallic Compound B-Ti(3)Au. *Science Advances* **2016**, *2*, No. e1600319.
(99) Erdogdu, Y.; Jian, T.; Lopez, G. V.; Li, W.-L.; Wang, L.-S. On the Electronic Structure and Chemical Bonding of Titanium Tetraauride: Tiau4 and Tiau4−. *Chem. Phys. Lett.* **2014**, *610−611*, 23−28.
(100) Miller, J. T.; Kropf, A. J.; Zha, Y.; Regalbuto, J. R.; Delannoy, L.; Louis, C.; Bus, E.; van Bokhoven, J. A. The Effect of Gold Particle Size on Auau Bond Length and Reactivity toward Oxygen in Supported Catalysts. *J. Catal.* **2006**, *240*, 222−234.
(101) Lu, T. F.; Wang, Y. S.; Tomko, J. A.; Hopkins, P. E.; Zhang, H. X.; Prezhdo, O. V. Control of Charge Carrier Dynamics in Plasmonic Au Films by Tiox Substrate Stoichiometry. *J. Phys. Chem. Lett.* **2020**, *11*, 1419−1427.
(102) Tomadin, A.; Brida, D.; Cerullo, G.; Ferrari, A. C.; Polini, M. Nonequilibrium Dynamics of Photoexcited Electrons in Graphene: Collinear Scattering, Auger Processes, and the Impact of Screening. *Phys. Rev. B: Condens. Matter Mater. Phys.* **2013**, *88*, No. 035430.
(103) Dong, S.; Pal, S.; Lian, J.; Chan, Y.; Prezhdo, O. V.; Loh, Z. H. Sub-Picosecond Auger-Mediated Hole-Trapping Dynamics in Colloidal Cdse/Cds Core/Shell Nanoplatelets. *ACS Nano* **2016**, *10*, 9370−9378.
(104) Hyeon-Deuk, K.; Kim, J.; Prezhdo, O. V. Ab Initio Analysis of Auger-Assisted Electron Transfer. *J. Phys. Chem. Lett.* **2015**, *6*, 244−249.
(105) Bastida, A.; Cruz, C.; Zuniga, J.; Requena, A.; Miguel, B. A Modified Ehrenfest Method That Achieves Boltzmann Quantum State Populations. *Chem. Phys. Lett.* **2006**, *417*, 53−57.
(106) Volobuev, Y. L.; Hack, M. D.; Topaler, M. S.; Truhlar, D. G. Continuous Surface Switching: An Improved Time-Dependent Self-Consistent-Field Method for Nonadiabatic Dynamics. *J. Chem. Phys.* **2000**, *112*, 9716−9726.
(107) Prezhdo, O. V. Mean Field Approximation for the Stochastic Schrodinger Equation. *J. Chem. Phys.* **1999**, *111*, 8366−8377.

https://dx.doi.org/10.1021/acs.jpcb.0c03030
J. Phys. Chem. B 2020, 124, 4326−4337

(108) Prezhdo, O. V.; Rossky, P. J. Evaluation of Quantum Transition Rates from Quantum-Classical Molecular Dynamics Simulations. *J. Chem. Phys.* **1997**, *107*, 5863−5878.
(109) Schwartz, B. J.; Bittner, E. R.; Prezhdo, O. V.; Rossky, P. J. Quantum Decoherence and the Isotope Effect in Condensed Phase Nonadiabatic Molecular Dynamics Simulations. *J. Chem. Phys.* **1996**, *104*, 5942−5955.
(110) Prezhdo, O. V.; Rossky, P. J. Relationship between Quantum Decoherence Times and Solvation Dynamics in Condensed Phase Chemical Systems. *Phys. Rev. Lett.* **1998**, *81*, 5294−5297.
(111) Jaeger, H. M.; Fischer, S.; Prezhdo, O. V. Decoherence-Induced Surface Hopping. *J. Chem. Phys.* **2012**, *137*, 22A545.
(112) Zhu, C. Y.; Nangia, S.; Jasper, A. W.; Truhlar, D. G. Coherent Switching with Decay of Mixing: An Improved Treatment of Electronic Coherence for Non-Born-Oppenheimer Trajectories. *J. Chem. Phys.* **2004**, *121*, 7658−7670.
(113) Akimov, A. V.; Long, R.; Prezhdo, O. V. Coherence Penalty Functional: A Simple Method for Adding Decoherence in Ehrenfest Dynamics. *J. Chem. Phys.* **2014**, *140*, 194107.
(114) Bedard-Hearn, M. J.; Larsen, R. E.; Schwartz, B. J. Mean-Field Dynamics with Stochastic Decoherence (Mf-Sd): A New Algorithm for Nonadiabatic Mixed Quantum/Classical Molecular-Dynamics Simulations with Nuclear-Induced Decoherence. *J. Chem. Phys.* **2005**, *123*, 234106.
(115) Subotnik, J. E. Augmented Ehrenfest Dynamics Yields a Rate for Surface Hopping. *J. Chem. Phys.* **2010**, *132*, 134112.

https://dx.doi.org/10.1021/acs.jpcb.0c03030
J. Phys. Chem. B 2020, 124, 4326−4337